Supplementary Material

Valleytronics of III-V solid solutions for thermoelectric application

Payam Norouzzadeh[1], Ali Shakouri[2], and Daryoosh Vashaee[11]

[1]Electrical and Computer Engineering Department, North Carolina State University, Raleigh, NC 27606, USA

[2]Birck Nanotechnology Center, Purdue University, West Lafayette, IN 47907, USA

A comprehensive simulation model based on the Boltzmann transport equation and the Callaway model[1] for thermal conductivity was presented in the article to calculate the thermoelectric characteristics of both $Al_xGa_{1-x}As$. and $Ga_xIn_{1-x}P$ materials. The details of our computational approach for $Al_xGa_{1-x}As$ can be found in ref. [2]. Here we describe our attempts and results to model the thermoelectric properties of $Ga_xIn_{1-x}P$. We optimized our model by fitting the empirical data of Hall electron mobility versus temperature and carrier concentration [3,4,5] as well as thermal conductivity versus both composition and temperature [6,7,8,9]. The resulted set of material parameters were used for both electrical and thermal properties calculations. Therefore, the model parameters were validated based on the main transport quantities. The input data to the model calculations were the band structure parameters, doping concentration, the range of temperature, and the composition. All calculations were based on three conduction energy bands. The determined model parameters for $Ga_xIn_{1-x}P$ are given in Tables I and II.

The values of the band related properties are given in Table I. These parameters were kept constant in all the calculations versus composition, carrier concentration and temperature. The second sets of parameters which are lattice dependent and directly affect the lattice thermal conductivity are presented in Table II. The primary step in our calculations is proving the robust evidences about reliability of our model to accurately predict the thermoelectric properties of $Ga_xIn_{1-x}P$ system and to obtain a satisfactory fit of the experimental data. In order to show this reliability, we made an effort to fit the previously reported data for $Ga_xIn_{1-x}P$ material including Hall electron mobility versus composition, thermal conductivity versus temperature, and thermal conductivity versus composition.

Figure S1-(a, b) present the experimental and calculated electron mobility versus temperature (for different doping concentrations) and doping concentration (at different temperatures) for InP, GaP,

---

[1] To whom correspondence should be addressed; Email: dvashae@ncsu.edu, Tel: (919) 530-9599

and $Ga_xIn_{1-x}P$. Figure S1-(c) depicts the experimental and calculated thermal conductivity versus temperature for GaP and $Ga_xIn_{1-x}P$. Figure S1-(d) illustrates the thermal conductivity of $Ga_xIn_{1-x}P$ versus x (Ga content). In all figures (except Figure S1-(d)), the experimental data are shown by symbols and the calculated results are displayed by solid lines. In Figure S1-(d), the symbols are Adachi's model calculations of the thermal conductivity versus x and solid line shows our calculations [7,8]. A comparison between the experimental and calculated values in all figures show good agreements, which evidences the reliability of the predicted properties of $Al_xGa_{1-x}As$ and $Ga_xIn_{1-x}P$.
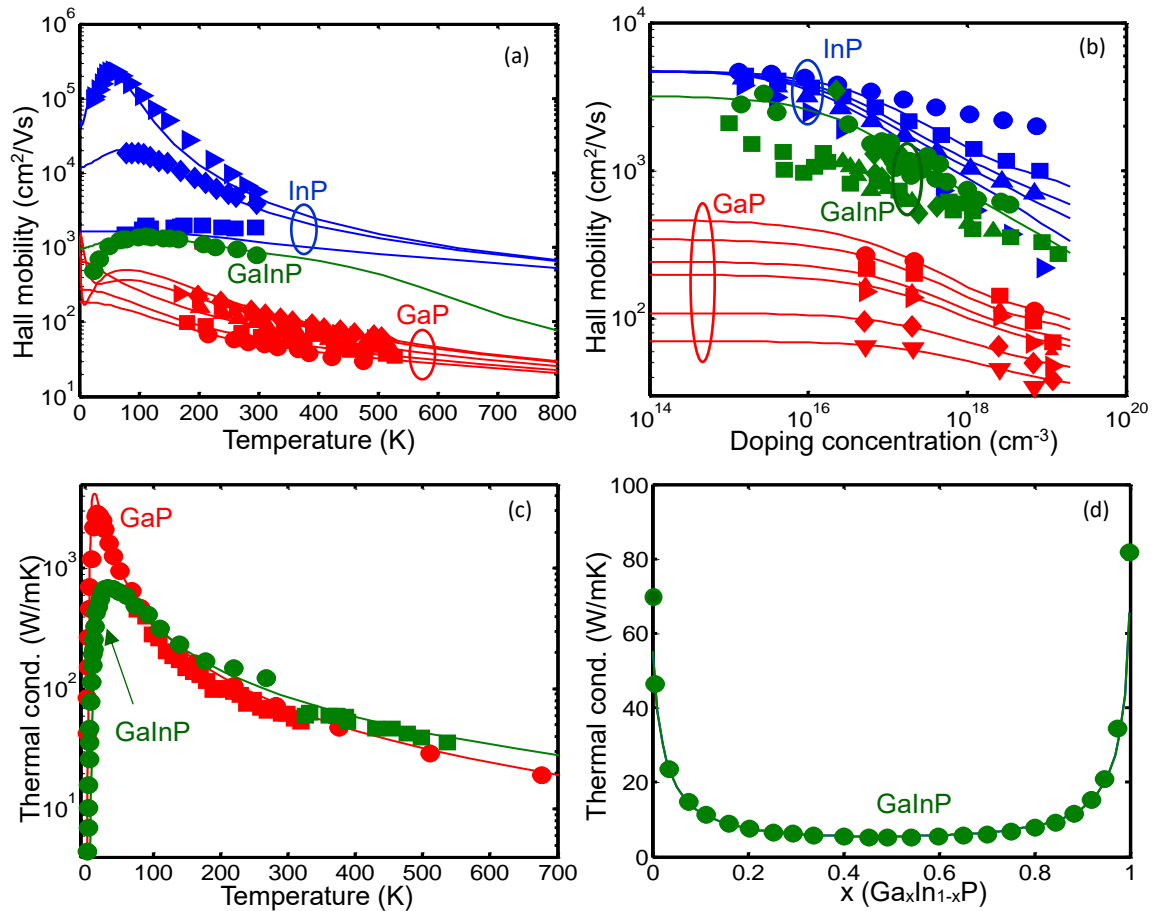

Figure S1: (a, b) The experimental (symbols) and calculated electron mobility (solid lines) for InP, GaP, and $Ga_xIn_{1-x}P$, respectively, versus temperature and doping concentration. (c, d) The experimental (symbols) and calculated (solid lines) lattice thermal conductivity of GaP and $Ga_xIn_{1-x}P$ versus temperature. (d) The calculated from ref [9, 10] (symbols) and our calculated (solid line) lattice thermal conductivity of $Ga_xIn_{1-x}P$ versus x.

Table I: Ga$_x$In$_{1-x}$P lattice parameters used to calculate the electrical conductivity

Parameter	Value	Reference
Static dielectric constant	13.18-3.12x	[10]
High frequency dielectric constant	11.6-3.44x	[10]
Bulk modulus (N/m^2)	(7.1+1.7x)×10^{10}	[9]
Mass density (kg/m^3)	4810-670x	[9]
Energy at Γ point	1.418+0.77x+0.648x^2	[11]
Energy at L point	1.958-0.019x+0.688x^2	[11]
Energy at X point	2.369-0.152x+0.147x^2	[11]
Conduction band (CB) effective mass at Γ for GaP	0.09	[9]
CB longitudinal effective mass at L for GaP	1.2	[9]
CB transverse effective mass at L for GaP	0.15	[9]
CB longitudinal effective mass at X for GaP	1.12	[9]
CB transverse effective mass at X for GaP	0.22	[9]
CB effective mass at Γ for InP	0.08	[9]
CB longitudinal effective mass at L for InP	0.25	[9]
CB transverse effective mass at L for InP	0.25	[9]
CB longitudinal effective mass at X for InP	0.32	[9]
CB transverse effective mass at X for InP	0.32	[9]
Valence band (VB) effective mass (heavy hole)	0.60+0.19x	[9]
VB effective mass (light hole)	0.089+0.051x	[9]
CB acoustic phonon deformation potential (eV)	5.1+7.6 x	[10]
VB acoustic phonon deformation potential (eV)	-5.1+17.8 x	[10]
Strain parameter for point defect scattering	20	[7]
CB acoustic phonon deformation potential (eV)	5.1+7.6x	[10]
VB acoustic phonon deformation potential (eV)	-5.1+17.8x	[10]
CB non-parabolicity (eV^{-1}) for L, Γ, X	0.5, 0.5, 0.5	This work
VB non-parabolicity (eV^{-1})	0.83	This work

Table II: Ga$_x$In$_{1-x}$P lattice parameters used to calculate the lattice thermal conductivity

Parameter	Value	Reference
Debye temperature (K)	301+144x	[9]
Bulk modulus (N/m^2)	(7.1+1.7x)×10^{10}	[9]
Mass density (kg/m^3)	4810-670x	[9]
CB acoustic phonon deformation potential (eV)	5.1+7.6x	[10]
VB acoustic phonon deformation potential (eV)	-5.1+17.8x	[10]
Strain parameter for point defect scattering	20	[7]
Grüneisen parameter	0.045+0.055x	This work
Higher order phonon scattering	3-0.4x	This work
Ratio of normal to Umklapp scattering	1.0	This work

I. Relaxation times

The scattering processes in a material are taken into account by relaxation times. Various approximations of the relaxation times can be found in the literature.[12,13] The relaxation times used here incorporate nonparabolicity of the band. The relaxation time for the ionized impurity scattering is given by following formula[12,13]

$$\tau_{ii}^{-1} = \left(\frac{\sqrt{2}e^4 N_I m_d^{\frac{3}{2}}}{\pi \varepsilon_s^2 \hbar^4}\right)\left(E(1+\alpha E)\right)^{\frac{1}{2}}(1+2\alpha E)\left(\frac{1}{q_D^2(q_D^2+\frac{8m_d E(1+\alpha E)}{\hbar^2})}\right) \tag{1}$$

where $q_D = \sqrt{\frac{N_I \varepsilon^2}{\varepsilon k_B T_L}}$.

The acoustic phonon scattering rate was calculated based on the effective deformation potential approximation.[14]

The scattering rates for equivalent and non-equivalent valleys for electron transfer from i to j valley are given, respectively, by the following relations:[15]

$$\tau_{iv}^{-1} = \frac{(Z_e-1)\left(m_j^*\right)^{\frac{3}{2}}D_{ij}^2}{\sqrt{2}\pi\rho\omega_{ij}\hbar^3}E_f^{\frac{1}{2}} \times \begin{cases} N & absorption \\ N+1 & emission \end{cases}$$

$$\text{in which} \quad E_f = \begin{cases} E + \hbar\omega_{ij} & absorption \\ E - \hbar\omega_{ij} & emission \end{cases} \tag{2}$$

$$\tau_{iv}^{-1} = \frac{Z_j\left(m_j^*\right)^{\frac{3}{2}}D_{ij}^2}{\sqrt{2}\pi\rho\omega_{ij}\hbar^3}\left[E_f\left(1+\alpha_f E_f\right)\right]^{\frac{1}{2}}(1+2\alpha_f E_f)G_{ij}\left(E_i, E_f\right) \times \begin{cases} N & absorption \\ N+1 & emission \end{cases} \tag{3}$$

in which G_{ij} is defined as $G_{ij}(E_i, E_f) = \frac{(1+\alpha_i E_i)(1+\alpha_f E_f)}{(1+2\alpha_i E_i)(1+2\alpha_f E_f)}$. Z_e, D_{ij}, ω_{ij}, ρ and E_f are the number of equivalent valleys, deformation potential, the phonon frequency which allows the intervalley scattering, density, and Fermi energy, respectively. In case of non-equivalent intervalley scattering, $Z_e - 1$ is replaced by Z_j which is the number of available final valleys for scattering.

The relaxation time τ_{DP} for acoustic phonon scattering is:[16]

$$\tau_0^{-1} = \frac{\pi k_B T D_A^2}{\rho v_s^2 \hbar}D(E), \qquad \tau_{ac}^{-1} = \tau_0^{-1}\{[1 - \frac{\alpha E}{1+2\alpha E}(1-\frac{D_v}{D_A})]^2 - \frac{8}{3}\frac{\alpha E(1+\alpha E)}{(1+\alpha E)^2}\frac{D_v}{D_A}\} \tag{4}$$

where E is the energy relative to the band edge, α is the nonparabolicity parameter, $D(E)$ is the density of states, ρ is the density, v_s is the sound speed, D_A and D_v are the conduction-band and valence-band deformation potentials, respectively. The values of the charge carrier deformational potentials used are listed in Table I.

The selected materials both are polar materials; so, we also calculated the polar longitudinal optical phonon scattering rates using the following relation:

$$\frac{1}{\tau} = \frac{4\pi\varepsilon_0\hbar}{3e^2 N_0}\left(\frac{1}{1/\varepsilon_\infty - 1/\varepsilon_0}\right)\sqrt{\frac{2\hbar}{m_{DOS}^*\omega_{op}\left(1+\hbar\omega_{op}\alpha\right)}}\frac{x+\beta x^2}{1+2\beta x} \tag{5}$$

Here $x = E/k_B T$ is the reduced energy, and $\beta = \alpha k_B T$ is the reduced non-parabolicity.

To obtain the total relaxation time, we applied the Matthiessen's rule:[12]

$$\frac{1}{\tau} = \frac{1}{\tau_{ii}} + \frac{1}{\tau_{iv}} + \frac{1}{\tau_{ac}}$$

(6)

II. The main thermoelectric properties

The formulas were used to calculate the electrical conductivity, Seebeck coefficient, and the electronic thermal conductivity as applied in a multiband model of Boltzmann transport theory. The electrical conductivity and Seebeck coefficient are given by:

,

$$\sigma = \frac{e^2 (2m_{DOS}^* k_B T)^{\frac{3}{2}}}{m_{nx} \pi^2 \hbar^3} \int_{x_f}^{\infty} \left(\frac{-\partial f_0}{\partial x}\right) \tau(x) \frac{(x + \beta x^2)^{3/2}}{1 + 2\beta x} dx$$

(7)

$$S = -\frac{k_B}{e} \left(\frac{\int_{x_f}^{\infty} \frac{\left(\frac{-\partial f_0}{\partial x}\right) \tau(x) x (x + \beta x^2)^{\frac{3}{2}}}{1 + 2\beta x} dx}{\int_{x_f}^{\infty} \frac{\left(\frac{-\partial f_0}{\partial x}\right) \tau(x) (x + \beta x^2)^{\frac{3}{2}}}{1 + 2\beta x} dx} - x_{Fermi} \right)$$

(8)

in which $\left(-\frac{\partial f_0}{\partial E}\right) = \frac{1/k_B T}{e^{(E-E_F)/k_B T} + 2 + e^{-(E-E_F)/k_B T}} = \frac{1/k_B T}{4\cosh^2((E-E_F)/2k_B T)}$

is the derivative of Fermi-Dirac distribution function, $x = E/k_B T$ is the reduced energy, $\beta = \alpha k_B T$ is the reduced non-parabolicity, and τ is the total scattering time. m_{nx} is the conductivity effective mass.[16] This procedure is repeated for each temperature, doping concentration, and different bands allowing all of the thermoelectric properties to be determined over the desired temperature and doping concentration ranges for each band. For the multiband transport model, the effective total electrical conductivity and Seebeck coefficient can be calculated as

$$\sigma_{tot} = \sum_i \sigma_i, \qquad S_{tot} = \frac{\sum_i \sigma_i S_i}{\sigma_i}$$

(9)

where σ_i and S_i are the electrical conductivity and Seebeck coefficients, respectively, for each individual band. The contribution of the carriers of different bands to the thermal transport is calculated using the Widemann-Franz law[17]

$$\kappa_e = \sum_i L_i \sigma_i T$$

(10)

in which T is the absolute temperature, and L_i, σ_i, are the Lorentz number, and the electrical conductivity, for each band. The Lorenz number is known to vary with the carrier concentration especially at low carrier concentrations, where L can be significantly lower than the free-electron value, so, we calculated L as function of carrier concentration using

$$L_i = \left(\frac{k_B}{e}\right)^2 \left\{ \frac{{}_2\varsigma_{-1}^{3/2}}{{}_0\varsigma_{-1}^{3/2}} - \left[\frac{{}_1\varsigma_{-1}^{3/2}}{{}_0\varsigma_{-1}^{3/2}}\right]^2 \right\}$$

(11)

where we have

$$\prescript{n}{k}{\zeta}_r^m = \int_0^\infty (-\frac{\partial f}{\partial x}) x^n (x + \beta x^2)^m \tau(x)^k (1 + 2\beta x)^r dx \qquad (12)$$

and the summation is achieved over all contributing bands. The bipolar thermal conductivity can be calculated as

$$\kappa_b = \frac{1}{2} T \sum_{i,j} \sigma_i \sigma_j (S_i - S_j)^2 \qquad (13)$$

where i, j are the valley indices, and S is the Seebeck coefficient.

III.   Thermal conductivity

The formalism introduced by Callaway[18] is used to calculate the lattice thermal conductivity:
$$k_l = k_1 + k_2 \qquad (14)$$

where k_1 and k_2 can be expressed as:

$$k_1 = CT^3 \int_0^{\theta/T} \tau_C(x) G(x) dx \qquad (15)$$

$$k_2 = CT^3 \beta I \qquad (16)$$

with

$$\beta = \frac{\int_0^{\theta/T} \frac{\tau_C(x)}{\tau_N(x)} G(x) dx}{\int_0^{\theta/T} \frac{\tau_C(x)}{\tau_N(x)\tau_R(x)} G(x) dx} \quad \text{and} \quad I = \int_0^{\theta/T} \frac{\tau_C(x)}{\tau_N(x)} G(x) dx$$

where

$$G(x) = \frac{x^4 e^x}{(e^x - 1)^2} \quad , \quad \frac{1}{\tau_C(x)} = \frac{1}{\tau_N(x)} + \frac{1}{\tau_R(x)} \quad , \quad x = \frac{\hbar \omega}{k_B T} \quad , \quad m = \frac{\hbar}{k_B} \quad , \quad C = \frac{k_B m^3}{2\pi^2 v} \qquad (17)$$

in which $\hbar$ and k_B are Planck's and Boltzmann constants, respectively. The phonon angular frequency, the phonon group velocity (sound velocity), Debye temperature and absolute temperature are indicated by ω, v, θ , and T, respectively. τ_C , τ_N and τ_U represent combined, N (resistive), and Umklapp relaxation times, respectively. The ratio of the Umklapp to normal mode scattering was set to 0.2 in our model.
Total thermal conductivity is given by:
$$k = k_l + k_e + k_b \qquad (18)$$
where k_l represents the lattice part of thermal conductivity, k_e indicates the electronic part of it and k_b is the bipolar contribution to the total thermal conductivity.
The contribution of the charge carriers to the thermal conductivity is calculated considering different bands:[19]
$$k_e = \sum_i L_i T \sigma_i \qquad (19)$$

$$L_i = (\frac{k_B}{e})^2 \left\{ \frac{^2_1\varsigma^{3/2}_{-1}}{^0_1\varsigma^{3/2}_{-1}} - [\frac{^1_1\varsigma^{3/2}_{-1}}{^0_1\varsigma^{3/2}_{-1}}]^2 \right\} \tag{20}$$

which the summation is done over all the involved bands where:

$$^n_k\varsigma^m_r = \int\limits_0^\infty (-\frac{\partial f}{\partial x}) x^n (x + \beta x^2)^m \tau(x)^k (1 + 2\beta x)^r dx \tag{21}$$

In the above mentioned equations k_B is the Boltzmann constant, $x = E/k_B T$ is the reduced energy, α and $\beta = (k_B T)\alpha$ are the non-parabolicity parameters, $\eta = E_f/k_B T$ is the reduced Fermi energy and $f(x) = 1/(e^{(x-\eta)} + 1)$ is the Fermi-Dirac distribution function. The factor $(1+2\beta x)$ is induced due to the energy dependency of the effective mass to the non-parabolic band.

The bipolar thermal conductivity is calculated according to: [19]

$$k_b = (\frac{k_B}{e})^2 \frac{\sigma_1 \sigma_2}{\sigma_1 + \sigma_2} (S_1 - S_2)^2 T \tag{22}$$

where 1 and 2 indices refer to electrons and holes.

IV. Optimum doping concentration

For the case of $Al_x Ga_{1-x} As$, at x<0.26, zT vs doping concentration has two peaks, the first one is in the 10^{19} cm^{-3} range and second one is in 10^{20} cm^{-3} range. In this range of x, the first zT peak is larger. At 0.26<x<0.4, zT vs doping concentration still has two peaks, but the second zT peak is larger. At x>0.4, zT vs doping concentration has only one peak. The optimum doping concentration for the two peaks are plotted in Figure S2S-a.

Figure S2: The optimum doping concentration versus composition for (a) $Al_x Ga_{1-x} As$ and (b) $Ga_x In_{1-x} P$.
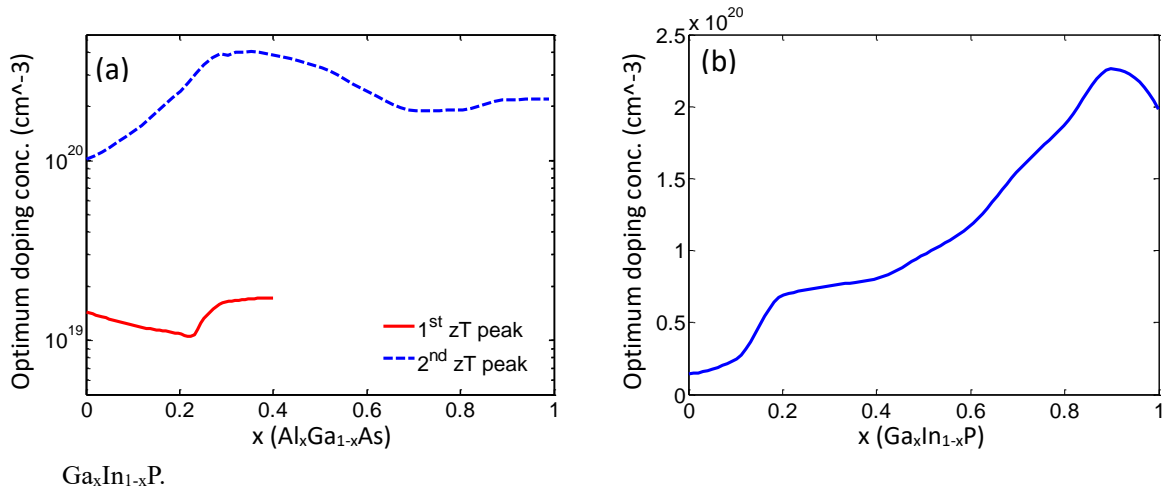
Also, for $In_{1-x} Ga_x P$, we calculated the optimum doping concentration for each x value, which is shown in Figure S2S-a.

V. Figure-of-merit versus composition

Figure S3 demonstrates the figure-of-merit versus composition for $Al_xGa_{1-x}As$ (panel (a)) and $Ga_xIn_{1-x}P$ (panel (b)). The zT calculations for fixed doping values of 1.05×10^{19} cm^{-3} and 1.5×10^{20} cm^{-3}, respectively, for AlGaAs and InGaP are also shown by dotted lines. In practice, it is difficult to reach doping in the range of high 10^{20} cm^{-3} in AlGaAs. Therefore, the 2nd zT peak for AlGaAs is difficult to reach. The calculated zT for the 1st peak is very close to the zT calculation assuming the fixed doping. Therefore, we reported the transport properties for a fixed practical doping concentration (~10^{19} cm^{-3}) for all the x values in the main manuscript.

It is evident that in GaInP the optimum doping curve has a negligible difference with the fixed doping curve. Therefore, the transport properties were reported for the fixed doping concentration of 1.5×10^{20} cm^{-3} in the main manuscript.
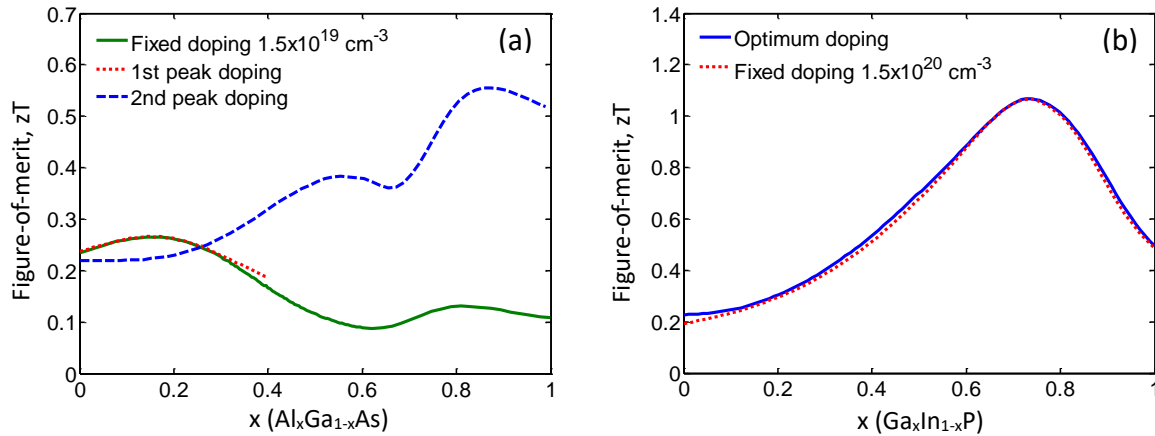

Figure S3: Figure-of-merit versus composition for (a) $Al_xGa_{1-x}As$ and (b) $Ga_xIn_{1-x}P$.

[1] J. Callaway, *Phys. Rev.* 113, 1046 (1959).
[2] P. Norouzzadeh, D. Vashaee, *J. Electron. Mater.* 44 (2), 636-644 (2015).
[3] Y. C. Kao and O. Eknoyan, *J. Appl. Phys.* 54, 5, 2468-2471 (1983).
[4] M. Razeghi, Ph. Maurel, M. Defour, F. Omnes, G. Neu, and A. Kozacki, *Appl. Phys. Lett.* 52, 2, 117-119 (1988).
[5] W. Walukiewicz, J. Lagowskii, L. Jastrzebski, P. Rava, M. Lichtensteiger, C. H. Gatos, and H.C. Gatos, *J. Appl. Phys.* 51, 5, 2659-2668 (1980).
[6] V. M. Muzhdaba, A. Ya. Nashelskii, P. V. Tamarin, and S. S. Shalyt, *Sov. Phys. Solid State* 10, 9, 2265-2267 (1968).
[7] S. Adachi, *J. Appl. Phys.* 54, 4, 1844-1848 (1983).
[8] S. Adachi, *J. Appl. Phys.* 102, 063502 (2007).
[9] The data of GaP and InP were taken from http://www.ioffe.ru/SVA/NSM/Semicond. The data for $Ga_xIn_{1-x}P$ were estimated using the weighted average of the properties of GaP and InP.
[10] The data of GaP and InP were taken from SpringerMaterials: The Landolt-Bornstein online database http://materials.springer.com/. The data for $Ga_xIn_{1-x}P$ were estimated using the weighted average of the properties of GaP and InP.
[11] D. Auvergne, P. Merle and H. Mathieu, Solid State Communications, Vol. 21, pp. 437-439, 1977
[12] M. Lundstrom, Fundamentals of Carrier Transport, 2nd ed., Cambridge University Press, Cambridge, (2000).
[13] J. Singh, Physics of Semiconductors and their Heterostructures, McGraw-Hill, Singapore, (1996).
[14] D. M. Zayachuk, Semiconductors 31, 2 (1997).
[15] J. Singh, Physics of semiconductors and their heterostructures, McGraw-Hill (1993).
[16] Yu. I. Ravich, B. A. Efimova, and V. I. Tamarchenko, Phys. Status Solidi B 43, 11 (1971).
[17] Thermoelectrics Handbook: Macro to Nano, edited by D. Rowe, CRC, Boca Raton, (2006).
[18] M. Asen-Palmer, K. Bartkowski, E. Gmelin, M. Cardona, A. Zhernov, A. Inyushkin, A. Taldenkov, V. Ozhogin, K. Itoh, E. Haller, Phys. Rev. B 1997, 56, 9431

[19] Y. Ravich, B. Efimova, and I. Smirnov, Semiconducting Lead Chalcogenides, 1970.